Rapid Communications

Commensurate-incommensurate phase transition of dense potassium simulated by machine-learned interatomic potential

Long Zhao,[1] Hongxiang Zong,[1,2,*] Xiangdong Ding,[1,†] Jun Sun,[1] and Graeme J. Ackland[2]
[1]*State Key Laboratory for Mechanical Behavior of Materials, Xi'an Jiaotong University, Xi'an 710049, China*
[2]*Centre for Science at Extreme Conditions (CSEC), School of Physics and Astronomy, University of Edinburgh, Edinburgh EH9 3FD, United Kingdom*

(Received 15 July 2019; published 2 December 2019)

The alkali metal potassium exhibits complex structures under pressure, including both commensurate and incommensurate phases, however, the transformation kinetics and microscopic mechanisms between these are yet to be elucidated. Here, we investigate the phase transformation behavior between close-packed fcc and incommensurate host-guest structures (KIII). We use multiscale molecular dynamics, with a machine-learned potential which fully reproduces the phase diagram and known phase transitions of potassium. We find that no straightforward, low-energy path exists: The previously proposed displacive transformation mechanisms have impossibly high kinetic barriers. The fcc-KIII transition occurs in a complex and diffusive manner, and involves an intermediate amorphization process during the nucleation of the product phase. Our findings may provide further insight into phase transition theory.

DOI: 10.1103/PhysRevB.100.220101

Solid-solid transitions are the most common types of structural phase transitions [1,2], and thus of central interest in metallurgy and crystallography [3–5]. Initial and final crystal orientations are often known, however, the transformation itself cannot be observed experimentally at the atomic level, which has resulted in many controversies over the underlying transformation pathways [6–8]. Elemental metals which crystallize in closely packed atomic arrangements, such as body-centered-cubic (bcc), face-centered-cubic (fcc), and hexagonal-closed-packed (hcp) [9,10], provide the simplest examples of solid-solid transitions. Their kinetic pathways often follow a displacive mechanism (characterized by atomic displacements within a unit cell) [11] or a diffusionless martensitic transformation with atoms moving in concert [9,12]. These pathways are strongly related to the symmetries of the parent and the product crystals [13–15]. It is found that the transitions may go through one or more intermediate metastable stages corresponding to common subgroups of the initial and final structures [16–19].

Temperature-driven transformations in pure elements are fairly rare, but under pressure most elements undergo a series of structural phase transitions that show diverse and sometimes unexpectedly complex structures [20–25]. Potassium (K) is an archetypal pressure-induced phase transforming material showing a complex phase diagram. It adopts the bcc crystal structure at ambient conditions, and on compression transforms to the fcc structure via a standard martensitic pathway [26]. Compressing further results in the emergence of complex incommensurate host-guest (h-g) structures (named KIII), which consist of two sublattices with one-dimensional (1D) atomic chain "guests" located in channels within a zeolite-type "host" structure. So far, experimental measurements [27–29] as well as density functional theory (DFT) calculations [30,31] have mainly focused on the thermodynamics, and crystal and electronic structures of host-guest structures. The microscopic kinetics of their transition pathways and associated mechanisms remain poorly understood, however, the tendency to form large crystals of KIII [32–34] suggests that the transformation is very slow. What is more, studying such a transition process is a challenging task since classic empirical potentials are not able to reproduce well the properties of both commensurate and incommensurate phases. On the other hand, nucleation is a rare event that occurs in much longer timescales than those achievable by *ab initio* molecular dynamics.

In this Rapid Communication, we use a combined machine-learning technique and atomic simulation approach to demonstrate that the microscopic kinetics of the closely packed fcc–incommensurate KIII transition in potassium occurs in a complex and diffusive manner, involving an intermediate disordering process by which the atomic displacement during the transition can exceed the unit cell length. This mechanism arises from the high entropy and the interfacial energy, which makes the pathway more favorable than energy-minimizing displacive mechanisms [35].

The interatomic interactions in potassium were described by a machine-learning interatomic potential (MLIP), which is based on high-throughput quantum-mechanical (QM) calculations [36,37]. In a previous work [38], we have shown that the MLIP can accurately describe all the different phases in the phase diagram, including the fcc and h-g. Additional information about the ML potential, in particular, the choice of combined descriptors for atomic environments and the learning set, is provided in the Supplemental Material [39].

*zonghust@mail.xjtu.edu.cn
†dingxd@mail.xjtu.edu.cn

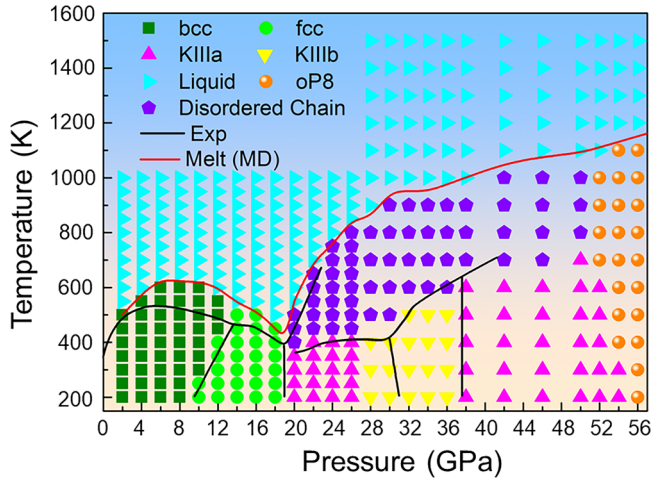

FIG. 1. MLIP predicted phase diagram of potassium. Each data point in this calculation represents an MD calculation (see Supplemental Material [39] for details) revealing the phase stability. Symbols show the various phases. Experimental phase boundaries for melting, chain melting, and solid-solid (black lines) are taken from Ref. [29].

Here, we utilized the ML potential to construct the potassium phase diagram. A series of molecular dynamics (MD) simulations on pressure-temperature grids with the *NPT* ensemble were used to find the stable structures, as shown in Fig. 1. At pressures below 20 GPa, the stable region of bcc and fcc lattices at low temperatures agrees with experiments and previous theoretical calculations [26,27]. The model also reproduces the melt line with a maximum and minimum by the *Z* method [52], at very similar pressures to those seen in experiment, and slightly higher temperatures. Between 20 and 44 GPa the simulations reproduce not only the h-g structures, but also the IIIa-IIIb-IIIa chain-ordering transformations, and the chain-melting phenomenon, in line with the experimental situation [31]. This interatomic potential with only one set of parameters captures the incommensurate host-guest structures and the pressure-temperature phase diagram of potassium, or indeed any other material with such a range of phases.

Since the MD simulation-based MLIP reproduces the phase stability, the microscopic kinetics of the fcc–h-g transition pathways can be investigated. The isothermal-isobaric (*NPT*) simulation of K single crystals starting from KIII lattices is first performed. Figure 2(a) shows the change in potential energy plotted as a function of simulation time for a typical MD trajectory at $T = 300$ K (which is 200 K below the melting temperature) and $P = 17$ GPa. We find the potential energy curve possesses a "double-step" profile. A close examination of the microstructure shows that the steps in the energy profile result from a two-step process of the nucleation. The first drop in the energy (∼137.3 meV/atom) is due to the formation of an intermediate structure. Then, the crystallization of fcc lattices occurs at the expense of these intermediate structures, giving rise to the second decrease of the potential energy (∼45.5 meV/atom). The simulation takes up to ∼220 ps for the entire KIII→fcc transformation to complete. Here, we note that it waits about 190 ps before the presence of an intermediate structure, indicating a high mechanically stable of the initial KIII structure.

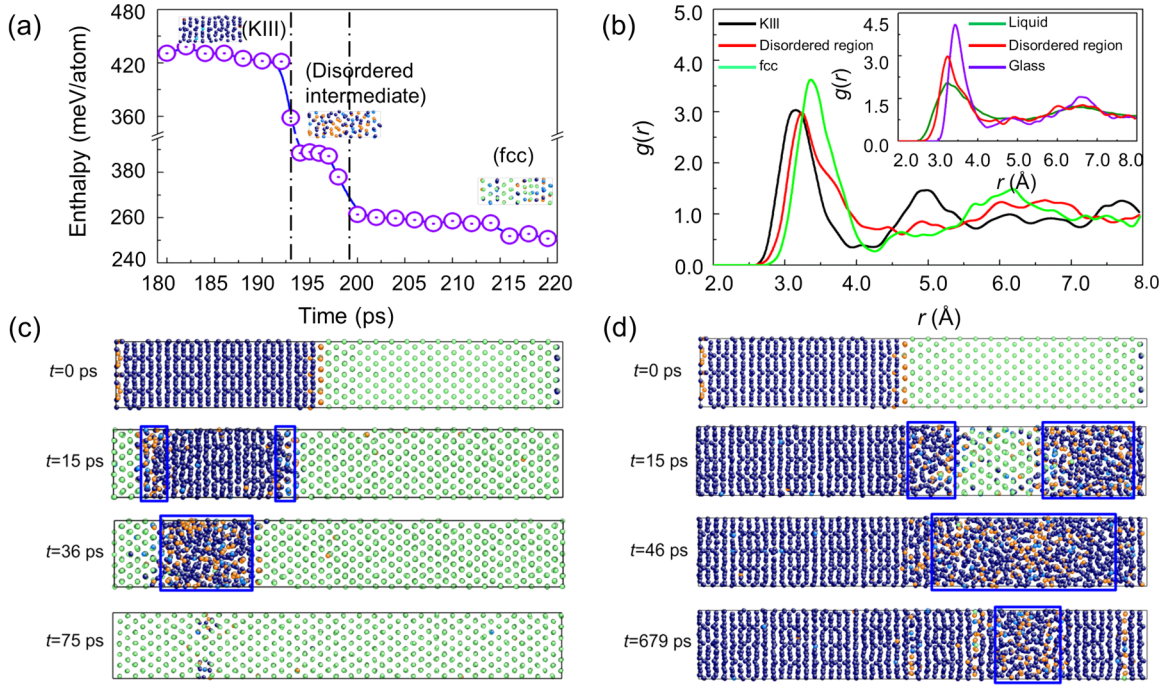

FIG. 2. Two-step phase transformation mechanism in potassium. (a) Potential energy changes during a typical MD simulation at 17 GPa, and snapshots indicating the transformation mechanism from KIII to fcc. (b) Radial distribution functions (RDFs) $g(r)$ of typical KIII, the disordered region, and fcc. The inset compares the RDFs of the disordered region, liquid, as well as a low-temperature amorphous solid. (c) and (d) Typical microstructure evolution of bicrystalline KIII-fcc upon isothermal annealing at 16 and 21 GPa. Blue boxes outline the presence of disordered regions.

The radial distribution functions (RDFs) $g(r)$ confirm that the phase transition involves a solid amorphization process. In Fig. 2(b), the $g(r)$ of the intermediate structure is quite different from either fcc or KIII, and it includes only one sharp peak at $R = 3.2$ Å. This lack of long-ranged order is characteristic of a liquid or solid amorphous material. A similar situation has been reported on bismuth experiments, which show a metastable liquid in the pressure-temperature region of supercooled liquid upon decompression from host-guest phases [19]. Therefore, we compared the $g(r)$ of the disordered region with that of a typical liquid as well as glass at the same pressures. As shown in the inset of Fig. 2(b), there was no significant difference among the three structures. However, we find that the disordering step of the KIII→fcc transition should not be a melting behavior but a solid amorphization process, evidenced by its existence even far below the supercooled liquid temperature region (Fig. S7, Supplemental Material [39]). To further demonstrate the effect, we applied phase-coexistence MD simulations using fcc-KIII interface models under both compression and decompression to confirm the existence of the two-step nucleation mechanism [Figs. 2(c) and 2(d)), and Figs. S5 and S6, Supplemental Material [39]]. Note that the intermediate amorphous structures on the KIII stability region show a survival time of up to subnanoseconds even with existing KIII embryos [Figs. 2(d) and S6(a)].

It is theorized that the formation of host-guest structures *could in principle* be achieved via a special displacive mechanism interpreted as resulting from the competition between the Burgers mechanism and Bain deformation [6], i.e., structural phase transformations that occur in a collective (shear/shufflelike) manner. To check whether this transformation *does in fact* occur via a displacive or martensitic character, the neighborhood of the K atoms before and after the transformation is investigated. Figures 3(a) and 3(b) show a cross section as well as its side view of atomic arrangements before and after the phase transitions that are obtained from three independent MD simulations. We find that few of the initial neighbor pairs remain as neighbors for both the forward and reverse phase transition. This indicates that atomic neighbor memories are destroyed during the transition and the transformation is not displacive, either for fcc-KIII or for KIII-fcc. Indeed, the three independent MD simulations show quite different atomic neighbors after the transitions despite using the same initial structure for the parent phase.

We define the overlap autocorrelation function as

$$\sigma(r,t) = \langle \delta_i(0,0) \cdot \delta_i(r,t) \rangle, \tag{1}$$

where r is the interatomic distance. This is a measure of the degree of atomic motion between two arbitrary configurations. Figures 3(c) and 3(d) show the radial part of $\sigma(r,t)$ during the forward and reverse fcc-KIII phase transition, respectively. The purple and light green curves represent the correlation function before and after the transition. The light green curve for $\sigma(r,t)$ shows that the transition is quite diffusive, as atoms move by up to ∼2.5 times the unit cell; this contrasts with typical martensitic transformations, such as the bcc-fcc transition with the same MLIP [Fig. 3(e)], where the atomic displacement is less than one unit cell.

Figure 4 compares the enthalpy barriers along the fcc-KIII transformation pathways between the proposed displacive

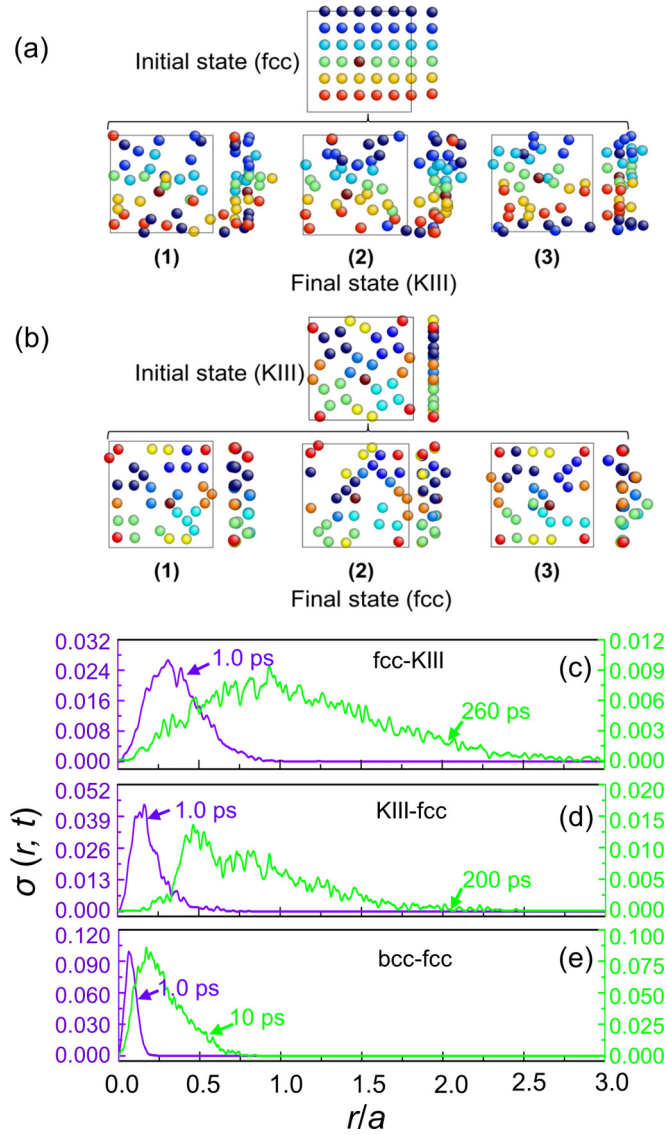

FIG. 3. Top view (in the box) and side view (to the right of the box) of the atomic arrangement of atoms starting in one fcc plane are labeled uniquely by their color. Initial and final states obtained from three independent MD simulations of (a) fcc→KIII and (b) KIII→fcc phase transitions. All memory of atomic neighbors is lost during the phase transition, and the side view shows that atoms move between planes. (c) and (d) show the corresponding autocorrelation function $\sigma(r,t)$ while (e) is the $\sigma(r,t)$) of the bcc → fcc martensitic transformation.

mechanism [35] and our two-step pathway. In the displacive mechanism, the KIII structure of potassium can be obtained from the fcc structure by antiparallel (±0.25,0,0) displacements combined with rotations of the square atomic motifs within the two layers [35], as shown in Fig. 4(a). Here, we adopted the same strategy of the nudged elastic band (NEB) algorithm that has been widely used to investigate the solid-solid phase transformations, which assumes that nuclear motion controls the phase transformation [53]. Figure 4(b) shows that the enthalpy change along the previously proposed displacive pathway [35] has a high barrier of ∼124.65 meV/atom at 20 GPa (the fcc-KIII transition pressure). For our

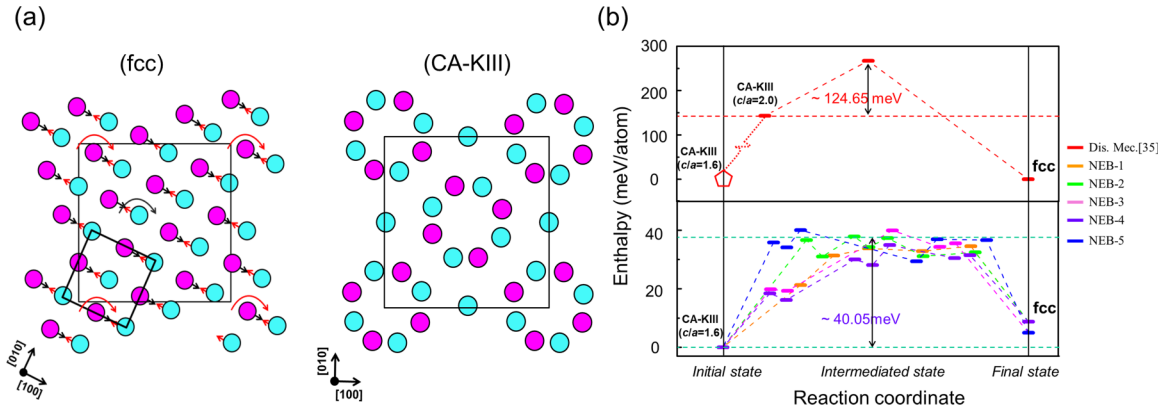

FIG. 4. (a) Illustration of the proposed displacive mechanism for fcc-KIII transition (pathway I), involving a displacement (arrows) and rotation (curved arrows) [35]. Atoms on different heights along z are labeled in different colors. (b) Enthalpy calculated along the two different transformation pathways. The CA-KIII represents the previously proposed mechanism [35], calculated with NEB, where the incommensurately modulated KIII structure is represented by a commensurate approximant. The IC-KIII-fcc transition has no unique path as the intermediate state is disordered. To sample the barrier along many possible paths, we ran MD simulations starting from the same KIII structures (initial state) and transforming to some permutation of the fcc structure (final state). These form the initial and final states for the NEB calculation of the transition pathway [53].

two-step nucleation mechanism, we find a long, flat barrier along the pathway due to the complex energy landscape of glassy structures (Fig. S9, Supplemental Material [39]) with a significantly lower energy barrier than the displacive one [the maximum barrier of five independent simulations is ~40.05 meV/atom, as shown in Fig. 4(b)].

As well as the low energy of the transition state, the interfacial energy assists in the formation of a transient metastable amorphous state during the fcc-KIII transformation. We calculated the interfacial energy (see Supplemental Material [39]) between the fcc and KIII structures, assuming the orientation relation required for the displacive transition ($\gamma_{\mathrm{KIII/fcc}} = 946.25\,\mathrm{mJ/m^2}$). However, the corresponding interfacial energies with an amorphous interlayer are so much lower that it is favorable to form a double interface,

$$\gamma_{\mathrm{KIII/amorph}}(232.80\ \mathrm{mJ/m^2}) + \gamma_{\mathrm{amorph/fcc}}(190.56\ \mathrm{mJ/m^2}) < \gamma_{\mathrm{KIII/fcc}}(946.25\ \mathrm{mJ/m^2}). \quad (2)$$

So even in classical nucleation theory, the transient amorphous state will appear at the phase boundary [16,19].

It has been proposed that in bismuth an intermediate liquid phase can facilitate transformations, and that high stress can also initiate melting [19,54]. Structural studies do not distinguish between liquid and amorphous, so we calculated the viscosity of the disordered material (see Supplemental Material [39] for details). This reveals that potassium can form a supercooled liquid down to 400 K, which is approximately the temperature of the melting-point minimum. At temperatures below this, the viscosity rises sharply, indicating a liquid-amorphous transition. We conclude that our intermediate phase is not liquid.

So far, the observed martensitic phase transformations have prevailed among monatomic metals [6]. The present work amounts to a convincing atomic simulation of a disordering process intermediated phase transformation in potassium. This disordering process should be different from that in compressed silicon/carbon with a strong directional bonding [54,55], whereas potassium is an excellent free-electron material and the vitrification of single-element metals should be notoriously difficult. Presumably, it is due to the much softer potential energy surfaces of alkali metals compared to most of the other metals, which can facilitate diffusion and increase the possibilities of more complex random pathways under high pressure.

In summary, we examined the phase transformation of a closely packed (fcc) to incommensurate h-g structure (KIII) in potassium under high pressure. The MLIP trained from *ab initio* data has allowed us to directly simulate the phase transition process. Although symmetry allows for a displacive mechanism, we find the pressure-driven transformation proceeding along a pathway which includes a disordering process.

The intermediate amorphous structure should be observable in a dynamic compression experiment using femtosecond laser pulses. Our simulation results of potassium bicrystals have indicated that there exists a competition between the amorphization process and the following crystallization of the product phase. During the fcc-to-KIII phase transition, the intermediate amorphous region can be large and last a significantly longer time [in the timescale of x-ray free-electron laser (XFEL) experimental measurements] due to the quite low crystallization rate of KIII [see Fig. 2(d)]. Our work has additional implications for such studies where the timescale of the transition matches the rate of the pressure increase: It may be that in the time it would take to form the incommensurate phase, the pressure has already increased into the stability regime of another phase, and the slow-forming phase may never be observed [56].

This work was supported by Key Technologies R&D Program (Grant No. 2017YFB0702401), the National Natural Science Foundation of China (Grants No. 51320105014, No. 51931004, and No. 51871177), the ERC grant "Hecate", and the 111 project 2.0 (Grant No. BP2018008).

[1] D. A. Porter, K. E. Easterling, and M. Y. Sherif, *Phase Transformations in Metals and Alloys* (CRC Press, Boca Raton, FL, 2008).

[2] R. P. Dias and I. F. Silvera, Science **355**, 715 (2017).

[3] S. H. Kirby, W. B. Durham, and L. A. Stern, Science **252**, 5003 (1991).

[4] T. Irifune, A. Kurio, S. Sakamoto, T. Inoue, and H. Sumiya, Nature (London) **421**, 806 (2003).

[5] W. F. Smith, *Principles of Materials Science and Engineering* (McGraw-Hill, New York, 1996).

[6] G. E. Duval and R. A. Graham, Rev. Mod. Phys. **49**, 523 (1977).

[7] K. Kadau, T. C. Germann, P. S. Lomdahl, and B. L. Holian, Science **296**, 1681 (2002).

[8] P. S. Branicio, R. K. Kalia, A. Nakano, and P. Vashishta, Phys. Rev. Lett. **96**, 065502 (2006).

[9] K. Bhattacharya, S. Conti, G. Zanzotto, and J. Zimmer, Nature (London) **428**, 55 (2004).

[10] L. Gao, X. D. Ding, H. X. Zong, T. Lookman, J. Sun, X. B. Ren, and A. Saxena, Acta Mater. **66**, 69 (2014).

[11] H. Katzke and P. Toledano, Phys. Rev. B **75**, 174103 (2007).

[12] Y. Song, X. Chen, V. Dabade, T. W. Shield, and R. D. James, Nature (London) **502**, 7469 (2013).

[13] P. A. Lindgard and O. G. Mouritsen, Phys. Rev. Lett. **57**, 2458 (1986).

[14] S. Scandolo, M. Bernasconi, G. L. Chiarotti, P. Focher, and E. Tosatti, Phys. Rev. Lett. **74**, 4015 (1995).

[15] F. Zipoli, M. Bernasconi, and R. Martonak, Eur. Phys. J. B **39**, 41 (2004).

[16] Y. Peng, F. Wang, Z. R. Wang, A. M. Alsayed, Z. X. Zhang, A. G. Yodh, and Y. L. Han, Nat. Mater. **4**, 101 (2015).

[17] W. K. Qi, Y. Peng, Y. L. Han, R. K. Bowles, and M. Dijkstra, Phys. Rev. Lett. **115**, 185701 (2015).

[18] J. Duncan, A. Harjunmaa, R. Terrell, R. Drautz, G. Henkelman, and J. Rogal, Phys. Rev. Lett. **116**, 035701 (2016).

[19] C. L. Lin, J. S. Smith, S. V. Sinogeikin, Y. Kono, C. Park, C. Kenney-Benson, and G. Y. Shen, Nat. Commun. **8**, 14260 (2017).

[20] M. I. McMahon, L. F. Lundegaard, C. Hejny, S. Falconi, and R. J. Nelmes, Phys. Rev. B **73**, 134102 (2006).

[21] M. I. McMahon and R. J. Nelmes, Chem. Soc. Rev. **35**, 1341 (2006).

[22] O. Degtyareva, V. V. Struzhkin, and R. J. Hemley, Solid State Commun. **141**, 164 (2007).

[23] Y. M. Ma, M. Eremets, A. R. Oganov, Y. Xie, I. Trojan, S. Medvedev, A. O. Lyakhov, M. Valle, and V. Prakapenka, Nature (London) **458**, 182 (2009).

[24] R. P. Dias, O. Noked, and I. F. Silvera, Phys. Rev. Lett. **116**, 145501 (2016).

[25] M. I. McMahon, O. Degtyareva, and R. J. Nelmes, Phys. Rev. Lett. **85**, 4896 (2000).

[26] X. Ou, Mater. Sci. Technol. **33**, 822 (2017).

[27] M. I. McMahon, R. J. Nelmes, U. Schwarz, and K. Syassen, Phys. Rev. B **74**, 140102(R) (2006).

[28] O. Narygina, E. E. McBride, G. W. Stinton, and M. I. McMahon, Phys. Rev. B **84**, 054111 (2011).

[29] E. E. McBride, K. A. Munro, G. W. Stinton, R. J. Husband, R. Briggs, H. P. Liermann, and M. I. McMahon, Phys. Rev. B **91**, 144111 (2015).

[30] G. Woolman, V. Naden Robinson, M. Marques, I. Loa, G. J. Ackland, and A. Hermann, Phys. Rev. Mater. **2**, 053604 (2018).

[31] M. Marques, G. J. Ackland, L. F. Lundegaard, G. Stinton, R. J. Nelmes, M. I. McMahon, and J. Contreras-Garcia, Phys. Rev. Lett. **103**, 115501 (2009).

[32] M. G. Gorman, A. L. Coleman, R. Briggs, R. S. McWilliams, D. McGonegle, C. A. Bolme, A. E. Gleason, E. Galtier, H. J. Lee, E. Granados *et al.*, Sci. Rep. **8**, 16927 (2018).

[33] M. G. Gorman, A. L. Coleman, R. Briggs, R. S. McWilliams, A. Hermann, D. McGonegle, C. A. Bolme, A. E. Gleason, E. Galtier, H. J. Lee *et al.*, Appl. Phys. Lett. **114**, 120601 (2019).

[34] A. L. Coleman, M. G. Gorman, R. Briggs, R. S. McWilliams, D. McGonegle, C. A. Bolme, A. E. Gleason, D. E. Fratanduono, R. F. Smith, E. Galtier *et al.*, Phys. Rev. Lett. **122**, 255704 (2019).

[35] H. Katzke and P. Toledano, Phys. Rev. B **71**, 184101 (2005).

[36] A. P. Bartok, M. C. Payne, R. Kondor, and G. Csanyi, Phys. Rev. Lett. **104**, 136403 (2010).

[37] P. Rowe, G. Csanyi, D. Alfe, and A. Michaelides, Phys. Rev. B **97**, 054303 (2018).

[38] V. N. Robinson, H. X. Zong, G. J. Ackland, G. Woolman, and A. Hermann, Proc. Natl. Acad. Sci. USA **116**, 10297 (2019).

[39] See Supplemental Material at http://link.aps.org/supplemental/10.1103/PhysRevB.100.220101 for details about the description and benchmark of the machine-learning interatomic potential, microstructure evolution during the fcc-KIII phase transition, as well as properties of intermediate disordered regions, which includes Refs. [40–51].

[40] G. Kresse and J. Furthmuller, Phys. Rev. B **54**, 11169 (1996).

[41] J. P. Perdew, K. Burke, and M. Ernzerhof, Phys. Rev. Lett. **77**, 3865 (1996).

[42] B. Schölkopf and A. J. Smola, *Learning with Kernels* (MIT Press, Cambridge, MA, 2002).

[43] T. Hastie, R. Tibshirani, and J. Friedman, *The Elements of Statistical Learning: Data Mining, Inference, and Prediction*, 2nd ed. (Springer, New York, 2009).

[44] S. Plimpton, J. Comput. Phys. **117**, 1 (1995).

[45] M. Parrinello and A. Rahman, J. Chem. Phys. **76**, 2662 (1982).

[46] M. Parrinello and A. Rahman, J. Appl. Phys. **52**, 7182 (1981).

[47] A. B. Belonoshko, N. V. Skorodumova, A. Rosengren, and B. Johansson, Phys. Rev. B **73**, 012201 (2006).

[48] W. G. Hoover, Phys. Rev. A **31**, 1695 (1985).

[49] M. P. Allen and M. R. Wilson, J. Comput.-Aided Mol. Des. **3**, 335 (1989).

[50] N. Meyer, H. Xu, and J. F. Wax, Phys. Rev. B **93**, 214203 (2016).

[51] J. C. Boettger, Phys. Rev. B. **53**, 13133 (1996).

[52] A. B. Belonoshko, L. Burakovsky, S. P. Chen, B. Johansson, A. S. Mikhaylushkin, D. L. Preston, S. I. Simak, and D. C. Swift, Phys. Rev. Lett. **100**, 135701 (2008).

[53] D. R. Trinkle, R. G. Hennig, S. G. Srinivasan, D. M. Hatch, M. D. Jones, H. T. Stokes, R. C. Albers, and J. W. Wilkins, Phys. Rev. Lett. **91**, 025701 (2003).

[54] J. Greeley, T. F. Jaramillo, J. Bonde, I. B. Chorkendorff, and J. K. Nørskov, Nat. Mater. **5**, 909 (2006).

[55] J. Behler, R. Martoňák, D. Donadio, and M. Parrinello, Phys. Rev. Lett. **100**, 185501 (2008).

[56] C. M. Pépin, A. Sollier, A. Marizy, F. Occelli, M. Sander, R. Torchio, and P. Loubeyre, Phys. Rev. B **100**, 060101(R) (2019).